Using Experimental Methods and Mathematical Modeling to determine Gap Junction Coupling in Neural Networks

Diana Martinez
Division of Biological Sciences,
Department of Mathematical Sciences
New Jersey Institute of Technology
dm62@njit.edu

Maciej Malej
Department of Mathematical Sciences,
New Jersey Institute of Technology
mm59@njit.edu

Angelie Mascarinas
Department of Biomedical Engineering,
New Jersey Institute of Technology
alm3@njit.edu

Submitted by: **Dr. Farzan Nadim**
and **Dr. Jorge Golowasch**

CAMS Report 0506-9, [Fall 2005/Spring 2006]
Center for Applied Mathematics and Statistics

I. Abstract

The existence of electrical synapses between neurons has been determined to play an important role in communication and network synchronization. The location of the gap junctional communication between neurons is of functional importance because of the complex neuronal morphology and the non-uniform distribution of voltage-gated ionic channels. However, accurately locating the gap junctions has been an elusive task. We performed intracellular recordings of two gap-junctionally coupled neurons in the crab Cancer borealis and examined signal transfer between these neurons using a variety of stimuli. We constructed a simplified mathematical model of the neurons to predict the location of the gap junctional coupling using the obtained experimental data.

II. Introduction

Electrical gap junctions are synapses that mediate the electrical communication between neurons. Gap junctions are formed by clusters of ion channels that span the plasma membrane of two neurons which therefore connect the neurons directly into their cytoplasmic compartment (Gibson et. al, 2005). Gap junctions are found in various locations such as between GABAergic inhibitory interneurons in the neocortex (Gibson et. al, 2005), in the retina of the eye (Dermietzel et. al. 2000), and in the synchronization of the respiratory pattern generator (Rekling et. al. 2000). Therefore, studying the location of gap junctions is important in order to fully understand their role in cell to cell communications.

Gap junctions or electrical synapses mediate a variety of cell to cell processes. Some examples of what is mediated through electrical synapses are: 1)burst formation in networks where there are no endogenously bursting neurons, 2)synchronizing the activity of a group of neurons, and 3)short latency and fast transmission in such networks as those that for escape reflexes (Johnson et. Al, 1993).They also play an important role in synchronizing the behavior and the output of neural networks. One such neural network is the one found in the Stomatogastric Nervous System of the Crab, *Cancer borealis.* Two cells in particular are found in the the Stomatogastric Nervous System of the Crab, *Cancer borealis*, the Pyloric dilator cells are connected through gap junctions. The PD cells are strongly coupled and are believed to be morphologically identical.

It is our hypothesis that the gap junction between these 2 cells can be located somewhere within the neuropil of the ganglion. Therefore, using varying experimental

methods the location of the gap junction between two electrically coupled cells must be determined.

During this study we used experimental data from the two pyloric cells of the Stomatogastric Nervous System to build a mathematical model. Recordings were done by injecting various levels static and dynamic current into one PD, and recording from the coupled PD as well as the first. Three electrodes were used, two into PD one (where recording and current injection takes place) in order to eliminate possible error from recording and injecting current through the same electrode. Alexa dyes were also used in order to visually determine the location of the gap junction. Alexa dyes do not cross gap junctions and therefore create a border between the two cells in question. A mathematical model was created by fitting parameters to experimental data and using this to determine gap junction location.

III. Methods:

Experimental

Experiments were conducted on the Jonah crab (*Cancer borealis*), purchased from Ocean Seafood (Newark, New Jersey) and were kept in artificial sea water tanks at a range of 12-15^{o}C until use. Anesthetization of the animals took about thirty minutes and was done using packed ice. The stomatogastric nervous system (STNS), with the STG (stomatogastric ganglion), the esophageal ganglion and commissural ganglion, was excised using standard methods (Harris-Warrick 1992). In order to allow for electrode access to the cells, the STNS was pinned to a Sylgard coated dish and the STG was desheathed. Superfusion of the preparation was done with physiological saline pH=7.4 and at a temperature range of 10-13^{o}C containing (in mM) 11.0 KCl, 440.0 NaCl, 13.0

$CaCl_2 \cdot 2H_2O$, 26.0 $MgCl_2 \cdot 6H_2O$, 5.1 Trizma base, and 5.1 Maleic acid. Microelectrodes with a resistance of 13-23 MΩ were pulled using a Flaming-Brown micropipette puller and filled with 6M KCl and 0.20 M KSO_4. Identification of the cells were done by matching the intracellular recordings with their corresponding extracellular recordings on motor nerves (Rabbah, Golowasch, Nadim 2005) After identification of the cells, the PDs were impaled with three electrodes, two electrodes were placed in the cell where current would be injected and one into the electrically coupled cell. The preparation was then superfused using 10^{-7} tetrodotoxin (TTX) to block inward sodium current, 100 mM Tetra-Ethyl-Ammonium (TEA) to block outward potassium current, 4 mM 4-Amino-Pyridine (4-A-P) to block I_A current and Cesium Chloride (CsCl) to block I_H current.

Current injections of varying degrees were used in testing the electrical coupling of the PDs. Beginning with hyperpolarizing 2nA stepwise current was injected into the first PD and recorded from both the first and second. This step required the use of three electrodes in order to correct for error from recording and injecting current from the same electrode. A change of 0.5 nA (ending at +0.5 nA) was applied each time and an average of five sweeps was taken in order to get an accurate view of the cells' behavior during stimulation. Sine waves of frequency in Hz, 1,2,5,10,20,50, and 100 were also injected into the PD.

In order to test the low pass filtering capabilities of these 2 electrically coupled cells, a ZAP function was injected. A ZAP, or Impedance (Z) amplitude profile, function is a signal that sweeps a variety of frequencies over time (Hutcheon & Yarom ,2000). Since impedance is frequency dependent between the amplitudes and phases of oscillatory signals, using a ZAP function is useful because each frequency can be isolated

in time in order for analysis (Hutcheon & Yarom ,2000). A ZAP function was created to last 210 seconds and scanned frequencies ranging from 0.1 to 50 Hz and 0.1 to 100 Hz.

Gap junction visualization was then done by using Alexa flour hyrdrazides, by Molecular Probes in Eugene Ohio. Glass electrodes, varying in resistance from 13MΩ-33MΩ, were then back filled with either 488 Alexa dye or 568 Alexa dye, each having a unique visualizing wavelength. The PD cells previously located during electrophysiological testing were then ionophoretically injected using a pulse of -40nA for alternating on/off 10 seconds. Preparations were then left overnight in order for dyes to travel through all of the neurites.

The STG was then fixed using 4% Paraformaldehyde in 0.1M PBS (pH=7.3-7.37) for twenty minutes. After fixing in 4% Paraformaldehyde, washes were done using 0.1M PBS every one hour for 3-6 hours. Images were then taken using Leicascope imaging software Leica 50.

Model:

Using XPP, (Ermentrout 2002), the integrations of the membrane and cable equations were performed, using the stiff method for solving differential equations with a time step of 0.05 ms. Two cables were modeled of length 1,100 μm and with 10 compartments each measuring 110 μm, in order to create compartments that are considered isopotential, to mimic the 2 PD neurons.

Using XPP increasing sinusoidal current injections were modeled ranging in varying increments from 1 to 100 Hz and varying current injections (1-4 nA). The gap junctional coupling location was also varied in position and strength along the modeled

cable (Rall et. al 1995). We therefore tested the amplitude of the current injected as well as the frequency of the inputted current.

The resistance of the gap junctional coupling (rc) of the 2 modeled neurons was varied to be $2x10^9\ \Omega$, $2x10^8\ \Omega$, $2x10^7\ \Omega$ and $2x10^6\ \Omega$. The gap junctional coupling location was also changed. Three different locations were chosen for the gap junctional coupling location. The first location modeled represented the third compartment of the cable, the second location modeled was the sixth compartment and the last position modeled was the ninth compartment out of the possible ten.

The cable equation governs the dynamics of the membrane potential in neuronal elongated processes such as axons or dendrites.

$$\tau_m \frac{\partial V m}{\partial t} = E - V + \lambda^2 \cdot \frac{\partial^2 V}{\partial x^2}$$

The equations were then discretized as seen from figure 1, utilizing passive membrane properties (discretizing the equation) in order to obtain passive properties of the cell. The membrane itself can be thought of as a two dimensional entity depending on the section that one chooses to analyze. This is due to the membrane properties such as the voltage gated channels as well as the varying membrane potential. An important merit of this linear partial differential equation, is that we are able to deal with on spatial dimension, namely the length of the cable.

Through discretization and compartmentalization of the cable equation a system of ordinary differential equations were derived. The cable of length 1100 μm was divided into ten compartments. Each compartment measured 110 μm, with resistance (ri) between

each of the compartments of the cable identical as seen in figure 2. In this study the presence of the secondary and tertiary neurites were ignored (Rabbah, et al. 2005).

The modeled equations contained varying parameters. Iext which is our injected current was injected in nA(s) such as that used in the experimental protocol; 1 nA was used in the modeling protocols. The entire input resistance (Rin) was experimentally averaged to be 5.11 MΩ,. This value was used even though in the model the secondary and tertiary neurites were ignored. The values and the parameters that were used can be seen in the table below:

Notation	Description	Value/Formula	Units
Rm	Membrane Resistivity	6.5	$k\Omega \cdot cm^2$
Ri	Axial Resistivity	0.06	$k\Omega \cdot cm$
rm	Membrane Resistivity for Unit Length	$\frac{Rm}{2\pi \cdot r \cdot l\_comp}$	kΩ
ri	Core Resistance per unit length	$\frac{Ri \cdot l\_comp}{\pi \cdot r^2}$	kΩ
l	Cable Length	0.11	cm
l_comp	Compartment Length	0.011	cm
Rc	Coupling Resistance	2,20,200,2000	MΩ
N	Number of Compartments	10	N/A
Cm	Membrane Capacitance	1	$\frac{\mu F}{cm^2}$
cm	Compartmental Capacitance	$Cm \cdot 2\pi r \cdot l\_comp$	μF
Iext	Injected Current	0.001	μA
Diameter	Cable Diameter	0.001	cm
R	Cable Radius	0.0005	cm
Vrest	Resting Potential	≈ –60	mV

The system of equations treats each compartment as an isopotential compartment, so that the membrane potential at each compartment is dependent on both the previous and subsequent compartment, leaky currents, as well as possible gap junctional coupling.

$$c_m \frac{dV_j^p}{dt} = I_j^p - \frac{V_j^p - V_{rest}}{r_m} - \underbrace{\frac{V_j^p - V_{j-1}^p}{r_i}}_{\text{Coupling to Prev. Compt.}} - \underbrace{\frac{V_j^p - V_{j+1}^p}{r_i}}_{\text{Coupling to Next Compt.}} - \underbrace{k(j)\frac{V_j^p - V_j^q}{r_c}}_{\text{Gap-junc. Coupling}}$$

The parameter K was chosen to be either 0 or 1, signifying turning on (1) or turning off(0) of the gap junctional coupling between the two parallel compartments. Therefore, we believe that the gap junctional coupling can only occur between two parallel compartments since it has been assumed that the 2 modeled neurons are morphologically identical. The superscripts *p* and *q* pertain to cable 1 (PD1) and cable 2 (PD2), respectively.

The zap function was also modeled between the 2 PD cells. ZAP allow the user to scan a variety of sinusoidal frequencies over a specific set time. The ZAP function used was identical to that of the experimental protocol scanning 0 to 100 Hz over a time period of 210 s.

Using the Clampfit program, various fits towards experimental episodic results were performed. Most of these fits were done using a linear combination of 2 exponential $V(t) = A_o e^{-\frac{t}{\tau_0}} + A_1 e^{-\frac{t}{\tau_1}}$ functions and the Levenberg-Marquardt method. In our fits τ_0 is believed to be the first prevailing time constant τ_m. The coupling coefficient can be correlated to the actual coupling strength of the gap junction under certain conditions such as coupling near the soma.

IV.Analysis/Results

Experimental

Using a data set of n=5, we used our experimental data to establish some of the parameters that would later be used in the model.

The time constants (τ) of the cells, which is the time it takes for the cell to attain 67% of its final voltage value, were analyzed by measuring the effects of stepwise current in PD2 in Clampfit. The τ is representative of the membrane resistance multiplied by the membrane capacitance $\tau = R_m C_m$. The data indicates that the time constant for PD1 ranged from 41.26 ms to 177.22 ms for the five data sets with a mean of 73.62 ms and a standard deviation of 45.63 ms. The time constant for PD2 ranged from 21.16 ms to 252.77 ms in our five data sets with a mean of 119.37 ms and a standard deviation of 48.62 ms.

The τ_0 and τ_1 of PD1 were then used to get the electrotonic length ,

L= $\frac{\pi}{\sqrt{\frac{\mathrm{To}}{\mathrm{T1}} - 1}}$. The data indicates that the electrotonic length (L) for PD1 ranged from 0.55 to 1.47 in our five data sets with a mean of 0.96 and a standard deviation of 0.36.

Coupling coefficients were then calculated by using the change of the voltage between both PDs and dividing by the larger changing voltage

$G = 100 - \left(\frac{\Delta V_{PD1} - \Delta V_{PD2}}{\Delta V_{PD1}} x100\% \right)$. Figure 3a shows that the coupling coefficients were determined to be between fifteen to forty percent. The change in voltage in PD1 for example with 1 nA step –wise current was between 4.73 to 10.31 mV. The change seen in PD 2 varied between 1.13 to 6.27 mV from the cell's resting membrane potential. The

coupling coefficient of the experimental data ranged from 14.04% to 42.15% with a mean of 25.52% and a standard deviation of 9.01%.

The input resistance of the biological data was calculated by using the equation $Rin = \frac{\Delta V_{PD1}}{I}$. The input resistances for our data ranged from 5.43 M Ω to 9.59 M Ω, with a mean of 6.77 M Ω with a standard deviation of 1.64 M Ω.

We performed various protocols using stepwise current, sine waves and zap waves, in order to estimate the location of the gap junctions and to further examine some of the properties of this gap junction. In one protocol, we used stepwise function which provided us with the parameters required to build our model. During experiments it was seen that both PD1 and PD2 after stimulation with a stepwise current returned back to their respective resting membrane potentials. PD2 showed a time delay, an average of 11 ms, from the current injection from PD1, as seen in figure 4a.

Phase shift dependence was calculated by injecting sinusoidal current into PD1 and recording from both PD1 and PD2. Phase shift was calculated by taking the difference in time between peaks of PD1 and PD2 and dividing by the period (1/frequency): $\phi = \frac{\Delta_{time} Peak_{PD1} - \Delta_{time} Peak_{PD2}}{Period}$. When looking at our data sets, a distinct pattern was seen as frequency increased. There is an exponential increase in phase shift that appears to level off as frequency increases. Figure 5a shows that when comparing the two nA sinusoidal current injection at frequency of 1 HZ to the two nA of 5 Hz, there is an obvious phase shift between the two PDs as well as the injected current.

The zap function which scans increasing sine frequencies over time allows for the analysis of the passive properties of the membrane. Injecting 0.1 Hz to 100 Hz, shows a

low pass filtering of the injected frequencies. The low pass filtering is a property of the cell's membrane where high frequencies are filtered out by the membrane's RC circuit capacity. There is attenuation between the reaction of PD 1 and PD2 when the zap is injected into the cell. Figure 6a demonstrates that as the frequencies increase, there is a greater fluctuation of current and consequently a decreasing amount of current that travels to PD2. The most dramatic attenuation, or low pass filtering, is seen beginning at 10 Hz, and only increases as time and frequencies progress.

Modeling

The cells that we used were considered passive for our mathematical model as well as for calculations. The model mimicked the use of TTX, TEA 4-A-P and CsCl in order to match the elimination of voltage gated channels as used in the experimental protocol. We used the obtained experimental parameters such as Rin, C, and Tau to better assimilate the model to the experimental findings.

The gap junctional coupling location of the model was varied. Alexa dye visualization also helped to physically demonstrate the locale of the gap junction. The two Alexa dyes create an area of convergence within the neuropil of the STG, and create a border between the locations of the two gap junctions. Therefore, the possibility that the gap junction could be located in or near the soma was eliminated. There we have assumed that the coupling is located within the neuropil of the stomatogastric nervous system of the crab. This assisted us in eliminating one position in the model and concentrating on three other possibilities compartment: 3,6 and 9 representative of the beginning, the middle and the end of the neurite.

After establishing the possible locations for the gap junctional coupling, we tested the three chosen locations while simultaneously testing the gap junctional resistances. The gap junctional coupling resistances were varied between 2 GΩ, 200 MΩ, 20 MΩ and 2 MΩ. As seen from figure 7a showing 2 GΩ as the gap junctional resistance, the first location was at compartment three which showed a phase shift of approximately 0.25 at 100 Hz, the second location was the sixth compartment which showed a phase shift of approximately 0.33 and the final location was compartment nine whose phase shift was found to be 0.37. Figure 7b, indicates that that with a change of gap junctional coupling to 200 MΩ and in comparison with the experimental phase shift there is still a significant difference between the strength and the locations. At compartment three there is a phase shift of 0.28, however at compartment six and nine 0.33 and 0.32 respectively. The gap junctional coupling resistance was then changed to 20 MΩ , and the gap junctional coupling location was also varied. At compartment three the phase shift was seen to be 0.22 , where compartments six the phase shift was 0.26 and 0.28 respectively. However, the strongest correlation was seen when the gap junctional coupling resistance was designated to be 2 MΩ and at compartment three where the phase shift was 0.165. Coupling at compartment six and nine with 2 MΩ of gap junctional coupling resistance was shown to be 0.23 and 0.27 respectively.

The amplitude ratio between PD1 and PD2 of the model was graphed as seen in figure 8b. The amplitude ratio was determined by dividing the change in membrane voltage of PD1 by the membrane voltage of PD2. The amplitude ratio between our modeled PD1 and PD2 subsequently increased with higher frequencies of sinusoidal current injections. The increase in amplitude ratio shows that PD2 is therefore receiving

a smaller amount of current from PD1. As the frequency of the sinusoidal current injection increases from 1 to 100 Hz, less current is passing through the resistive branch of the membrane circuit, because there is less current also being accumulated to charge the capacitor. Therefore, regardless of the current amplitude that is being injected into the model system, the response is still the same.

Comparison of Model and Experiment

Using the 2MΩ model with a gap junctional coupling location of the third compartment, we compared both experimental and modeling data obtained from the stepwise stimulations that we injected. As seen from figure 4, the experimental data and model give similar results, where the voltage of experimental PD2 being attenuated by 1.88 mV while the model gave a change of 1.98 mV.

Using the experimental data we compared the electrotonic length for PD1 from the model in both the 2 MΩ and 20 MΩ coupling resistances with coupling at compartment. We found that with a hyperpolarizing stepwise injection of 1nA, the electronic length for PD1 of the model was 0.63 for the 2 MΩ and 1.63 for the 20 MΩ. As seen from figure 9, the experimental data gave a mean of 0.96 with a standard deviation of ±0.36.

When the coupling coefficient of the episodic stimulations in both the model and experiment were compared, there was a large difference seen between the modeled 2 MΩ and 20 MΩ gap junctional coupling resistances with coupling at compartment 3. The coupling coefficient at 2 MΩ coupling resistance was 40% while the 20 MΩ was 70%. It is important to note that the coupling coefficient is only an approximation of coupling strength when measuring from the soma as opposed to directly at the coupling site.

However, the method of recording from the soma as in the experimental protocol, was mimicked in the model. As seen in figure 3, the experimental data are closer to the modeled 20 MΩ gap junctional resistance rather than that of the 2 MΩ resistances.

Sine waves were then injected in varying frequencies. As seen from the data, there was a time delay between the PD2, PD1 and current injection. PD2 was considerably shifted with increasing frequencies. Since we have treated this with pharmacological agents, creating a "nearly passive" cell system, it was simpler to analyze the details of why this occurs. As the frequencies of the sine wave increase, there is a greater attenuation of the current and consequently the cell is receiving less and less current to charge the capacitive branch. Since the membrane acts as an RC circuit, it is dependent on both the capacitive and resistive branches of current. Therefore, the faster the frequency the less time available to charge the capacitor thus going to the resistive factor of the membrane creating a low pass filtering effect in both the model and experiments. This in essence causes a "short circuiting" of the membrane system (Johnson &Wu .

When comparing the sinusoidal input of the model to that of the experimental we were able to eliminate one of the parameters. As seen from figure 8, we were able to eliminate amplitude variations on the overall affect of the phase shift. The experimental data shows that as frequency increased the phase shift also increased, however amplitude of the injected sine wave did not impact the overall phase shift results. Therefore, our model, also correlated with the experimental results and we were able to eliminate amplitude as a variable and determine that phase shift dependent primarily on frequency of the injected sinusoidal current. In the model and the experiments, amplitudes were

varied between one, two and four nA, yet we were able to see that regardless of the amplitude injected in both the model and the experiments, there was no effect on the phase shift.

Because we have established that sinusoidal current amplitude injection is not a relevant parameter when comparing the phase shifts, we were able to concentrate on comparing only frequency of the inputted current and the location and strength of the gap junctional coupling. We have previously established in this paper that gap junctional coupling at compartment three is the best fit to the experimental data. As seen in figure 10, when the location of the coupling was fixed at compartment three we compared the various gap junctional coupling strengths. When compared to the experimental data it is shown that the 2 MΩ modeled gap junction most closely resembles the experimental data obtained. As gap junction location is kept constant and junctional resistance is increased, there is a greater discrepancy between the experimental data and the model.

When comparing phase shift between PD1 and PD2 with the obtained modeled curves we can determine which curve best fits the experimental data. Taking the average error between the acquired data from the model we were able further correlate that the gap junctional coupling location at compartment three and the gap junctional resistivity of 2 MΩ best fits the experimental data. As seen in figure 11, the average error was determined to be 38% between the modeled and experimental data and its resistance of approximately 2 MΩ.

When comparing the ZAP functions for both the experimental data and the modeled cell, we found that the 2 M Ω gap junctional coupling resistance was the best fit. As seen from figure 6, when injecting a ZAP of 1nA and 0.1-100 Hz over 210 s , we saw

that both were correlated. The low pass filtering effect was seen in both the modeled and experimental data due to the RC filtering effect of both.

V. Discussion

Gap junctions are formed by clusters of ion channels that span the plasma membrane of two neurons which therefore connect the neurons directly into their cytoplasmic compartment (Gibson et. Al, 2004). Their location and their function can vary from organism to organism. It is therefore necessary to understand the function of the gap junctions and their actions on cells within a system.

Gap junctions function in a variety of ways dependent on location and strength. In mammals, gap junctions help to produce a synchronized patterned output, such as in the respiratory central pattern generator (Rekling et. al. 2000). Another example of the importance of gap junctions is seen in the supraoptic neurons that are believed to generate circadian rhythms. Gap junctions are also found in the hippocampal region and make dendrodentritic connections (Fukuda,2000). It is suggested that they function in controlling the oscillations of the GABAergic interneurons (Kosaka, 1983). Abnormalities in gap junction proteins have also been found to be an indicator of certain types of cervical cancers (Cao, 2005). Formation of gap junctions also appears to allow the metastasis of breast cancer tumor and epithelial cells (Carystinos et. al 2001). Alterations in gap junctions in the astrocytes of the central nervous system are also shown to be a prominent feature in the demyelination that is found with Multiple Sclerosis (Brand-Scheiber ,2005). Thus, knowing the location of the gap junction and how it mediates the passage of current and controls oscillatory networks can possibly lead to the further understanding of other biological phenomena. Using the stomatogastric system of

the crab as a model network, allows for the study of the gap junctions for further research to higher animal systems.

Even though we set out to formulate the location of the gap junctions using the aformentioned protocols, further research is needed. We were able to rule out the soma as the location of the gap junction through visualization. We concluded, that the gap junctional coupling is best suited in the vicinty of the third compartment, with an optimal coupling resistance to be between 2 and 20 MΩ. Possible further areas of study include eliminating any factors that may hinder the establishment of the gap junction position. The PDs within the stomatogastric nervous system are also electrically coupled to the anterior burster neuron (AB) which can also have an effect on the output when stimulated with inputed current. By eliminating the AB experimentally, there would be a more accurate correlation between the model which only accounts for the PD neurons. Also by using more pharmological agents to block more currents, we can determine the strength and coupling better. In this model we simplified the structure of the PD neuron to a single cable with 10 compartments while excluding the secondary and tertiary neurites. However, the morphology of the PD neuron is much more complex. Perhaps also mimicking the secondary and tertiary neurites of the PDs would give a more accurate gap junctional location and strength. Finally the full consideration and analysis on the nonlinear system would be recommended without the reservation to the simplicity of the linear model.

Works Cited:

Bou-Flores, C. & Berger, A. J. (2001) *J. Neurophysiol.* **85**, 1543-1551

Brand-Scheiber E , Werner P, Iacobas DA, Iacobas S Connexin43, the major gap junction protein of astrocytes, is down-regulated in inflamed white matter in an animal model of multiple sclerosis. J Neurosci Res 2005;.

Cao YW, Lu TC, Pan XL, Li F, Zhong HH, Sun Y, Jiang JF, Li L. Correlation of expression of connexin to growth and progression of cervical carcinoma in situ. Ai Zheng. 2005 May;24(5):567-72.

Carystinos GD, Bier A, Batist G: The role of connexin-mediated cell-cell communication in breast cancer metastasis. J Mammary Gland Biol Neoplasia 2001, 6:431-440.

Dermietzel R, Kremer M, Paputsoglu G, Stang A, Skerrett IM, Gomes D, Srinivas M, Janssen-Bienhold U, Weiler R, Nicholson BJ, Bruzzone R, Spray DC.," Molecular and functional diversity of neural connexins in the retina" J Neurosci. 2000 Nov 15;20(22):8331-43.

Ermentrout B. Simulating, analazing, and animating dynamical systems: a guide to XPPAUT for researchers and students (software, environment, tools). Philadelphia: Society for Industrial and Applied Mathematics, 2002.

Fukuda T, Kosaka T.. Gap junctions linking the dendritic network of GABAergic interneurons in the hippocampus. J Neurosci. 2000 Feb 15;20(4):1519-28.

Gibson J., Beirlein M., Connors B., Functional properties of electrical synapses between inhibitory interneurons of neocortical layer 4. J Neurophysiol. 2005 Jan;93(1):467-80.

Harris-Warrick RM, Nagy F, Nusbaum MP Neuromodulation of stomatogastric networks by identified neurons and transmitters. In: Dynamic Biological Networks: The Stomatogastric Nervous System (Harris-Warrick RM, Marder E, Selverston AI, Moulins M, eds), pp 87-138. Cambridge, MA: MIT Press. 1992

Hutcheon B, Yarom Y. Resonance, oscillation and the intrinsic frequency preferences of neurons. Trends Neurosci. 2000 May;23(5):216-22

Johnson BR, Peck JH, Harris-Warrick RM Amine modulation of electrical coupling in the pyloric network of the lobster stomatogastric ganglion. J Comp Physiol [A] 172:715-732. 1993

Johnson, D. & Wu, S. M.-S. (1995) *Foundations of Cellular Neurophysiology* (MIT Press, Cambridge, MA).

Kosaka T (1983): Axon initial segments of the granule cell in the rat dentate gyrus: Synaptic contacts on bundles of axon initial segments. *Brain Res* **274**:129-134

Rabbah P, Golowasch J, Nadim F. Effect of electrical coupling on ionic current and synaptic potential measurements. J Neurophysiol. 2005 Jul;94(1):519-30. Epub 2005 Feb 23.

Rall, W., Segev, I., Rinzel, J & Shepherd, G.M(1995) The Theoretical Foundation of Dendritic Function: Selected Papers of Wilfred Rall with Commentaries MIT Press, Cambridge, Massachusetts

Rekling JC, Shao XM, Feldman JL. Electrical coupling and excitatory synaptic transmission between rhythmogenic respiratory neurons in the preBotzinger complex. J Neurosci. 2000 Dec 1;20(23):RC113.

Traub, R., Pais I, Bibbig A., LeBeau F., Buhl E., Hormuadi S., Monyer H., Whittington M., "Contrasting roles of axonal (pyramidal cell) and dendritic (interneuron) electrical coupling in the generation of neuronal network oscillations" PNAS, February 4, 2003 ,vol. 100 , no. 3 , 1370-1374

Acknowledgements

This work was supported by NSF grant #0436244.

We would like to thank Nickolas Kintos and Vahid Tohidi for their patience and help during this project.

Figure	Legend
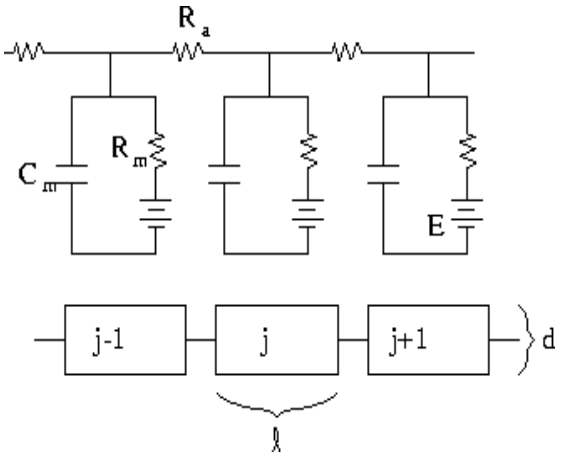	Figure 1:A discretization lets us treat the cable/neurite as a series of RC circuits. Discretization of the cable, then allows each cable to be treated as a series of isopotential compartments.
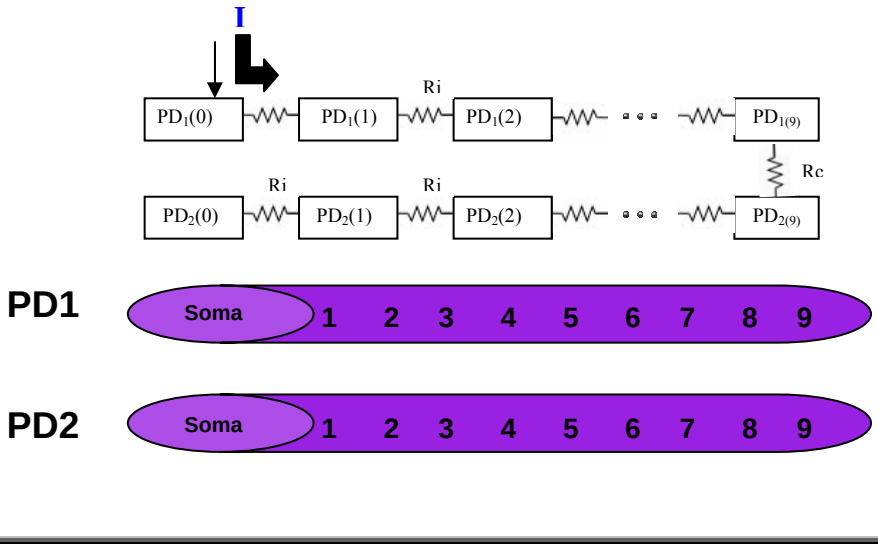	Figure 2: Neuronal cable schematic used for creating model. I represents current injected into the soma of PD_1. $PD_1(0)$ represents the soma for the first modeled neuron . $PD_1(n)$, where n=[1,9] represents the compartments adjacent to $PD_1(0)$. $PD_2(0)$ represents the soma for the second neuron. $PD_2(n)$, where n=[1,9] represents the compartments adjacent to $PD_2(0)$. The cable of the length 1100 µm used in the model contained 10 compartments 0-9. Each compartment is isopotential and only measure 110 µm.

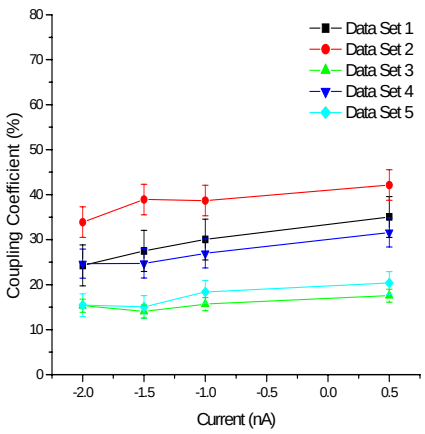

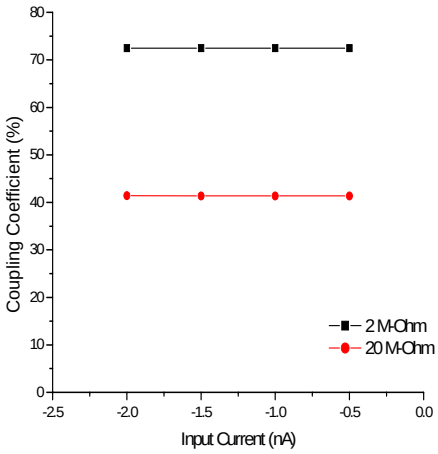

Figure 3: Comparison of the coupling coefficients of the model and experimental data. The coupling coefficient is determined by:

$$G = 100 - \left(\frac{\Delta V_{PD1} - \Delta V_{PD2}}{\Delta V_{PD1}} x100\% \right)$$

3a: The experimental data (n=5), ranged from 14.04% to 42.15% with a mean of 25.52% and a standard deviation of 9.01%.
3b: The modeled 2 MΩ and 20 MΩ resistances were modeled in order to compare to the experimental data. The 2 MΩ gave a resistance of close to 75% , while the 20 MΩ was closer to the experimental data.

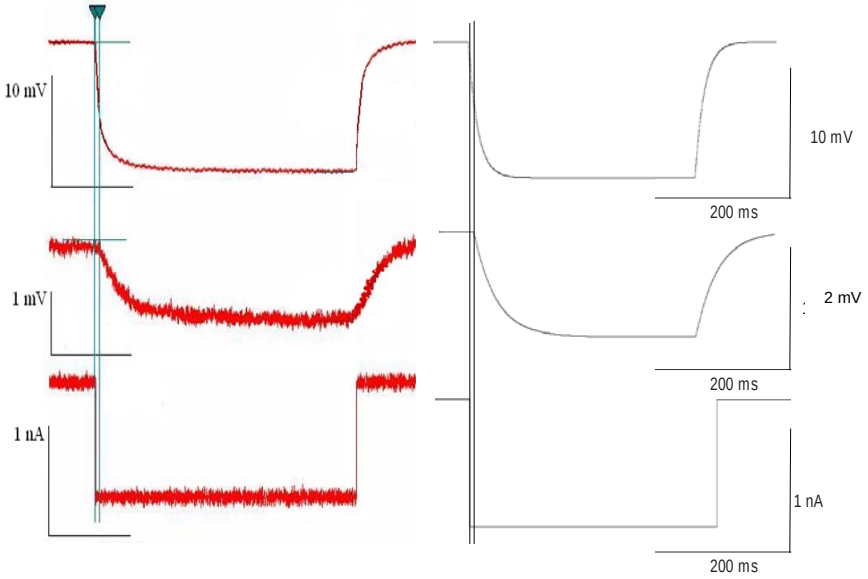

Figure 4: Comparison of episodic stimulations in both the model and experimental traces
4a: The experimental data shows that there is a difference in the attenuation of PD1 and PD2. With an injection of 1nA of hyperpolarizing current, there is a 11ms time delay between the response of PD1 and PD2. The experimental traces on the left gave a voltage change of -10.31 for PD1 and -1.88 mV.
4b: In the traces from the 2 MΩ model on the right there is a voltage change of -11.3 mV in PD1 and -1.98 mV in PD2.

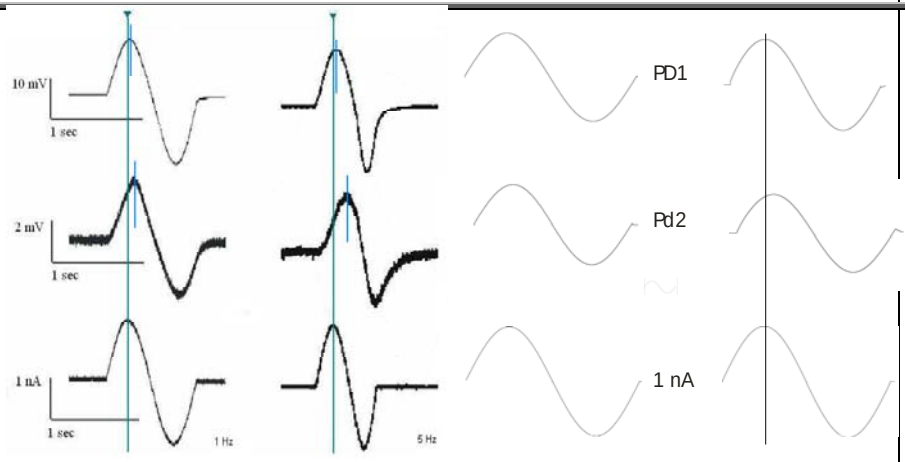

Figure 5: Comparing Sinusodial Current injection of 1nA at 1 and 5 Hz in both the model and experimental
5a: The trace on the left shows the experimental 1 Hz with very little phase shift. However, the trace on the right shows that increasing the frequency to 5 Hz gives a more defined phase shift.
5b: Results in the 2 MΩ model with a gap junctional coupling location of third compartment gave results similar to those of the experimental data.

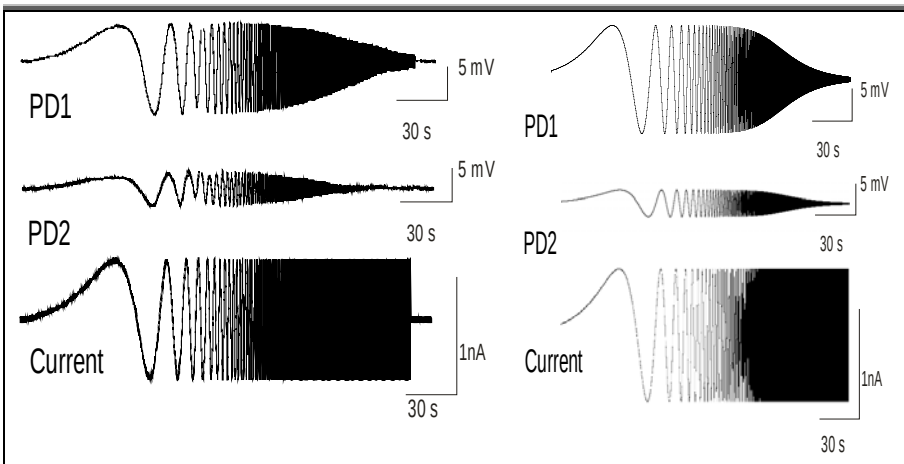

Figure 6: Comparing the ZAP function in the experimental data and the model
6a: Injecting 1 nA of current in 210 seconds showed a low pass filtering starting at 10 Hz. As frequencies increase there is a sharper and more well defined filtering in PD2.
6b: Injecting 1 nA of current in to the 2 MΩ with a gap junctional coupling location of the third compartment gave very similar results to those seen in the experimental.

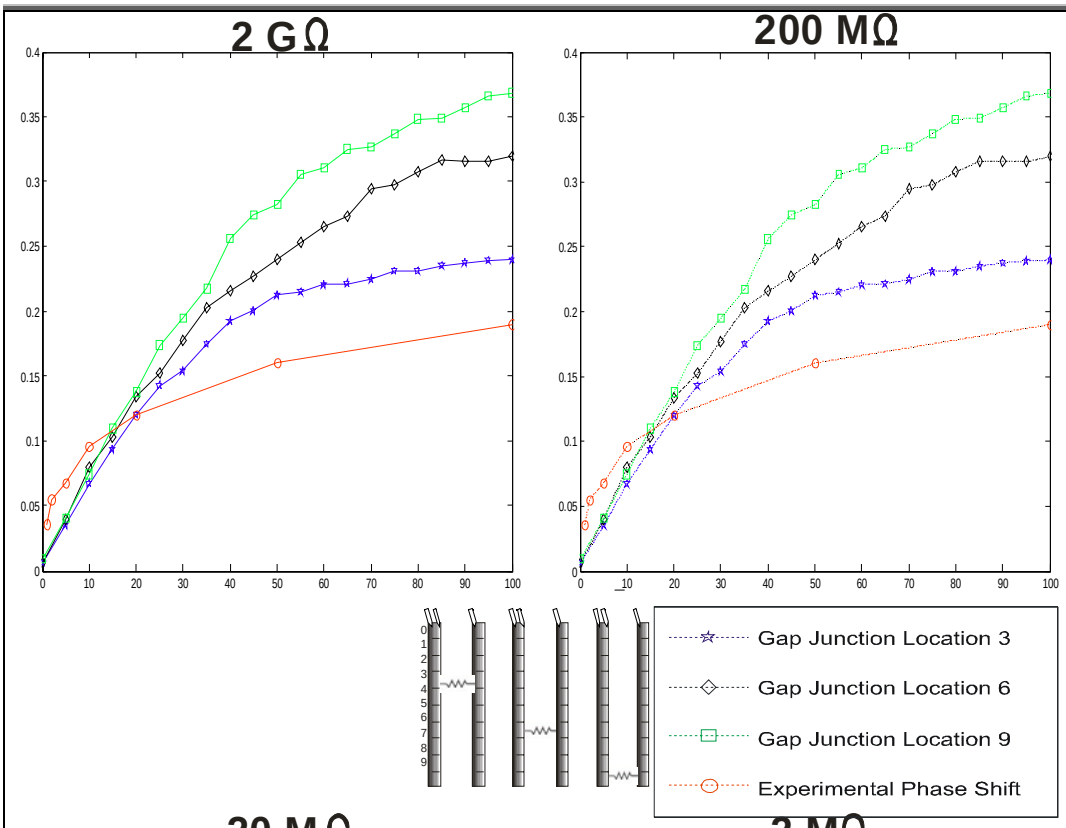

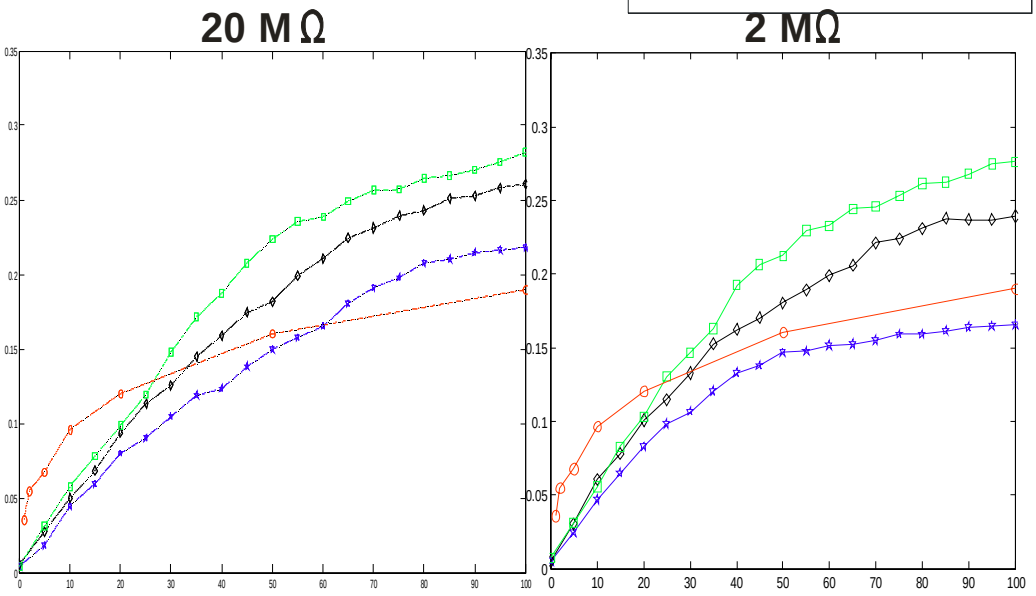

Figure 7: As the gap junctional coupling resistance was varied from very strong to a weaker resistance there is a strong correlation to the experimental result. In figure 7a, the gap coupling resistance was 2 GΩ. In figure 7b, the gap coupling resistance was changed to 200 MΩ. In figure 7c, gap coupling resistance was changed to 20 MΩ . In figure 7d, gap coupling resistance of 2 MΩ was the closest to the experimental data.

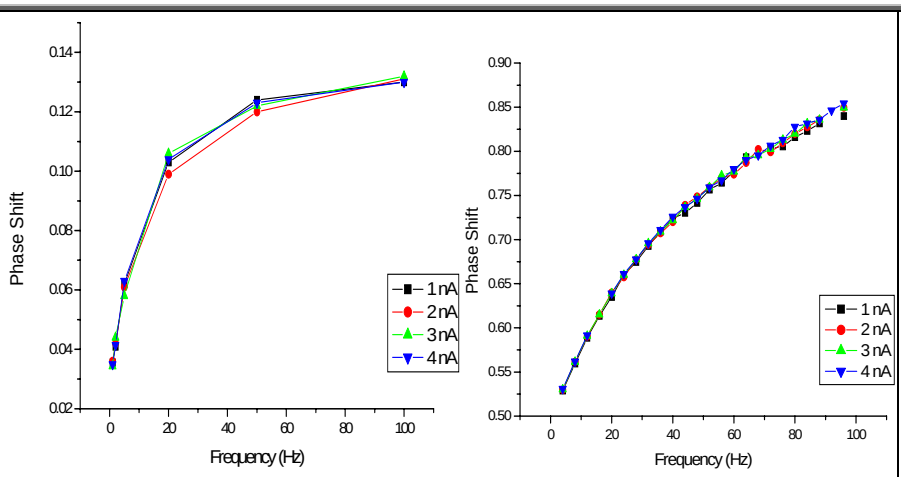

Figure 8: Comparing the Amplitude ratio of PD1 and PD2 in the model and experimental data. The amplitude ratio was determined by dividing the change in membrane voltage of PD1 by the membrane voltage of PD2.
8a: Experimental: With increasing frequency sinusoidal injection, regardless of the amplitude of the injected current, the phase shift resembles an asymptotic behavior with increasing frequency.
8b: The amplitude ratio between our modeled PD1 and PD2 subsequently increased with higher frequencies of sinusoidal current injections. As seen in the experimental data, regardless of the amplitude of the injected current, the phase shift resembles an asymptotic behavior with increasing frequency.

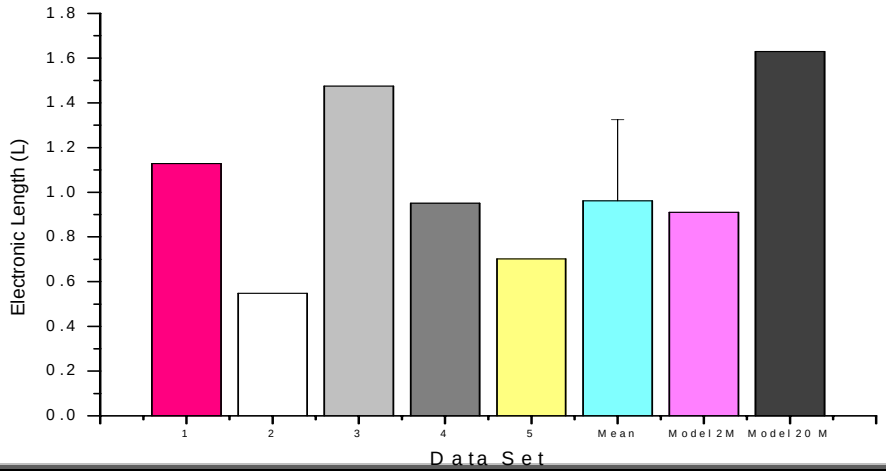

Figure 9: With hyperpolarizing stepwise injection of 1nA, the electrotonic length for PD1 of the model was 0.63 for the 2 MΩ and 1.63 for the 20 MΩ. The experimental data gave a mean of 0.96 with a standard deviation of ±0.36. The mean of the data and the modeled 2 MΩ gap junctional coupling resistance were the closest.

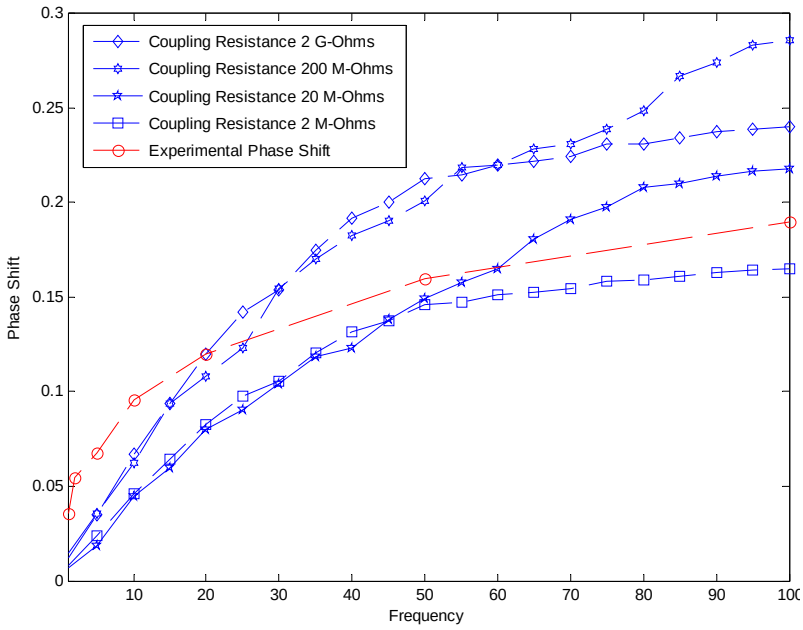

Figure 10: Keeping the gap junctional coupling location constant and varying the strength shows that the experimental data is directly related to the 2 MΩ gap junction resitivity. As gap junction location is maintained constant and the gap junctional resitivity increased there is greater variation between the experimental phase shift and the modeled phase shift.

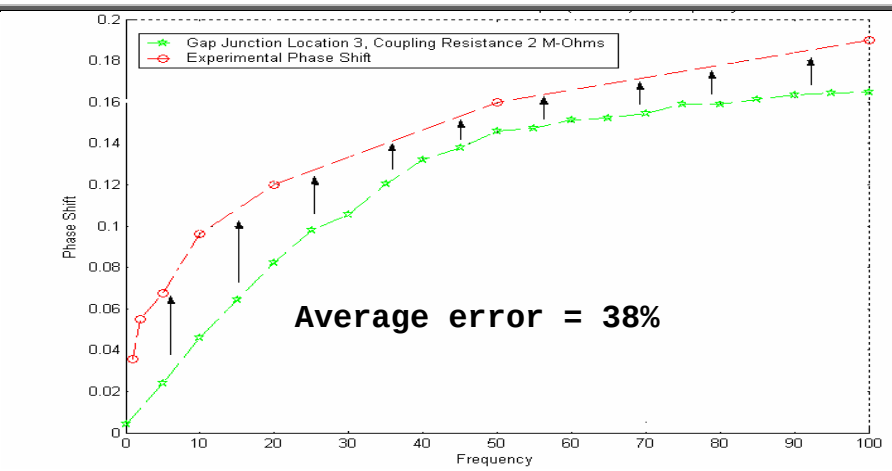

Figure 11: Comparing the phase shift between the 2 Mega-Ω model and the experimental gave the smallest average error with 38. %. Therefore, we can say that the gap junctional resistance is closest to 2 MΩ